

UC San Diego

UC San Diego Previously Published Works

Title

A genetically encoded far-red fluorescent calcium ion biosensor derived from a biliverdin-binding protein.

Permalink

<https://escholarship.org/uc/item/37h2d2b6>

Journal

Protein Science, 31(10)

Authors

Ota, Keisuke
Qian, Yong
Zhu, Wenchao
[et al.](#)

Publication Date







2022-10-01

DOI

10.1002/pro.4440

Peer reviewed

A genetically encoded far-red fluorescent calcium ion biosensor derived from a biliverdin-binding protein

Rina Hashizume¹ | Hajime Fujii² | Sohumi Mehta³  | Keisuke Ota² |
 Yong Qian^{4,5}  | Wenchao Zhu¹ | Mikhail Drobizhev⁶ | Yusuke Nasu¹  |
 Jin Zhang³  | Haruhiko Bito²  | Robert E. Campbell^{1,4} 

¹Department of Chemistry, School of Science, The University of Tokyo, Bunkyo-ku, Tokyo, Japan

²Department of Neurochemistry, Graduate School of Medicine, The University of Tokyo, Bunkyo-ku, Tokyo, Japan

³Department of Pharmacology, University of California San Diego, La Jolla, California, USA

⁴Department of Chemistry, University of Alberta, Edmonton, Alberta, Canada

⁵McGovern Institute for Brain Research, MIT, Cambridge, Massachusetts, USA

⁶Department of Microbiology and Cell Biology, Montana State University, Bozeman, Montana, USA

Correspondence

Yusuke Nasu and Robert E. Campbell,
 Department of Chemistry, School of
 Science, The University of Tokyo,
 Bunkyo-ku, Tokyo, Japan.
 Email: nasu@chem.s.u-tokyo.ac.jp (Y. N.)
 and campbell@chem.s.u-tokyo.ac.jp
 (R. E. C.)

Funding information

Astellas Foundation for Research on
 Metabolic Disorders; Canadian Institutes
 of Health Research; Hitachi Global
 Foundation; Japan Society for the
 Promotion of Science, Grant/Award
 Numbers: 19H05633, 17K13270,
 22H05160; Kato Memorial Bioscience
 Foundation; Nakatani Foundation for
 Advancement of Measuring Technologies
 in Biomedical Engineering; National
 Cancer Institute, Grant/Award Number:
 R01 DK073368; National Institute of
 Neurological Disorders and Stroke,
 Grant/Award Number: U24 NS109107;
 Natural Sciences and Engineering
 Research Council of Canada; National
 Institutes of Health; Montana State
 University; University of Alberta;
 University of California, San Diego;
 Takeda Science Foundation; Toyota
 Physical and Chemical Research Institute;
 University of Tokyo; Japan Agency for
 Medical Research and Development,
 Grant/Award Number: 19dm0207079

Abstract

Far-red and near-infrared (NIR) genetically encoded calcium ion (Ca^{2+}) indicators (GECIs) are powerful tools for in vivo and multiplexed imaging of neural activity and cell signaling. Inspired by a previous report to engineer a far-red fluorescent protein (FP) from a biliverdin (BV)-binding NIR FP, we have developed a far-red fluorescent GECI, designated iBB-GECO1, from a previously reported NIR GECI. iBB-GECO1 exhibits a relatively high molecular brightness, an inverse response to Ca^{2+} with $\Delta F/F_{\min} = -13$, and a near-optimal dissociation constant (K_d) for Ca^{2+} of 105 nM. We demonstrate the utility of iBB-GECO1 for four-color multiplexed imaging in MIN6 cells and five-color imaging in HEK293T cells. Like other BV-binding GECIs, iBB-GECO1 did not give robust signals during in vivo imaging of neural activity in mice, but did provide promising results that will guide future engineering efforts.

Significance: Genetically encoded calcium ion (Ca^{2+}) indicators (GECIs) compatible with common far-red laser lines ($\sim 630\text{--}640$ nm) on commercial microscopes are of critical importance for their widespread application to deep-tissue multiplexed imaging of neural activity. In this study, we engineered a far-red excitable fluorescent GECI, designated iBB-GECO1, that exhibits a range of preferable specifications such as high brightness, large fluorescence response to Ca^{2+} , and compatibility with multiplexed imaging in mammalian cells.

Hajime Fujii, Sohumi Mehta, and Keisuke Ota contributed equally to this study.

Review Editor: Aitziber Cortajarena

KEYWORDS

bacterial phytochrome-derived fluorescent proteins, calcium ion imaging, far-red fluorescence, protein engineering

1 | INTRODUCTION

The calcium ion (Ca^{2+}) is a secondary messenger that plays a central role in essentially all signaling activities in mammalian cells. Accordingly, genetically encoded Ca^{2+} indicators (GECIs; also known as biosensors) are important tools for monitoring a wide variety of biological signalling processes.¹ The majority of currently available GECIs are engineered versions of canonical β -barrel fluorescent proteins (FPs) that are homologs of *Aequorea* green FP (GFP) and are excitable by visible light (~ 400 – 600 nm).² The wavelengths of fluorescence excitation and emission peaks of these GECIs fall in the visible range of spectrum, which can limit their utility for deep-tissue imaging and for multiplexed imaging with other visible-colored probes. In contrast, far-red (~ 600 – 650 nm) and near-infrared (NIR; ~ 650 – 900 nm) wavelengths penetrate further through animal tissue because such wavelengths are less scattered and less absorbed by biomolecules.³ Moreover, fluorophores that are excited by far-red or NIR light are spectrally orthogonal to fluorophores excited by visible light and therefore provide new opportunities for multiplexed imaging.⁴

In an effort to overcome the limitations of existing visible-wavelength GECIs, we have previously developed first and second generation NIR fluorescent GECIs, designated NIR-GECO1, 2, and 2G (Figure 1a).^{4,5} The NIR-GECO proteins are based on the biliverdin (BV)-binding, bacterial phytochrome-derived, monomeric infrared FP (mIFP)⁶ with an inserted fusion of calmodulin (CaM) and the CaM-binding peptide of smooth muscle myosin light chain kinase (RS20). When bound to a phytochrome scaffold, BV shows two absorption peaks: one in the far-red region at 640–680 nm (Q-band), and another in the violet region at 370–400 nm (Soret band). Excitation of protein bound BV at these regions produces fluorescence in the NIR region at 650–710 nm. Upon excitation in the Q-band, members of the NIR-GECO series exhibit inverse Ca^{2+} -dependent fluorescence changes ($\Delta F/F_{\min} = [F_{+\text{Ca}} - F_{-\text{Ca}}]/F_{+\text{Ca}}$) as large as -15 and molecular fluorescent brightness up to 65% that of the mIFP parent protein (Table S1). Furthermore, we have demonstrated that NIR-GECO1 is applicable to multiplexed Ca^{2+} imaging in both cultured mammalian cells and primary neurons,⁴ and NIR-GECO2 (and 2G) is applicable to in vivo imaging in *Caenorhabditis elegans* and *Xenopus laevis*.⁵

An important consideration for practical and widespread application of a fluorescent probe is how well the optimal excitation wavelength is matched to common laser lines on commercial microscopes. In the far-red region, the helium-neon laser at 633 nm, and semiconductor lasers at ~ 640 nm, are commonly used for confocal microscopy. Unfortunately, the excitation peak of the NIR-GECO-series proteins (678 nm) is ~ 40 nm too long, meaning that excitation with the most commonly available laser lines does not provide the maximum fluorescence brightness of these indicators. To address this shortcoming, Subach and coworkers have undertaken the development of alternative NIR fluorescent GECIs, including GAF-CaMP2-sfGFP and GAF-CaMP3-sfGFP.^{7,8}

While these GECIs are more effectively excited with ~ 640 nm laser light, exhibit a preferable direct response to Ca^{2+} , and their maximum in vitro Ca^{2+} -dependent $\Delta F/F_{\min}$ is 2.3, they require cells to be supplemented with BV (20 μM) in order to observe far-red fluorescence, and their maximum fluorescence brightness is about half that of the NIR-GECO2 series members. In other work, Verkhusha and coworkers reported a Förster resonance energy transfer (FRET)-based ratiometric Ca^{2+} biosensor, designated iGECI, with an excitation peak at 640 nm.⁹ While benefiting from substantially improved brightness due to the use of the relatively bright mIFP670 donor, the Ca^{2+} -dependent $\Delta R/R$ of iGECI is limited to ~ 0.6 .

To develop an improved NIR fluorescent GECI with optimal excitation in the far-red region (~ 640 nm), we undertook the engineering of a blue-shifted version of NIR-GECO2. Our strategy for blue-shifting the fluorescence spectrum was inspired by the previously reported development of the blue-shifted iBlueberry variant (excitation maximum at 644 nm; emission maximum at 667 nm) from mIFP (excitation maximum at 683 nm; emission maximum at 704 nm).¹⁰ Unfortunately, the initial blue-shifted variants had greatly diminished responsiveness to Ca^{2+} . Recovery of the Ca^{2+} responsiveness was achieved through an extensive process of directed evolution that ultimately produced a variant designated iBB-GECO1, which has similar brightness and Ca^{2+} responsiveness to NIR-GECO2. We demonstrate that iBB-GECO1 has a number of favorable properties that make it particularly well suitable for multiplexed, multi-color imaging of Ca^{2+} dynamics in cultured cells.

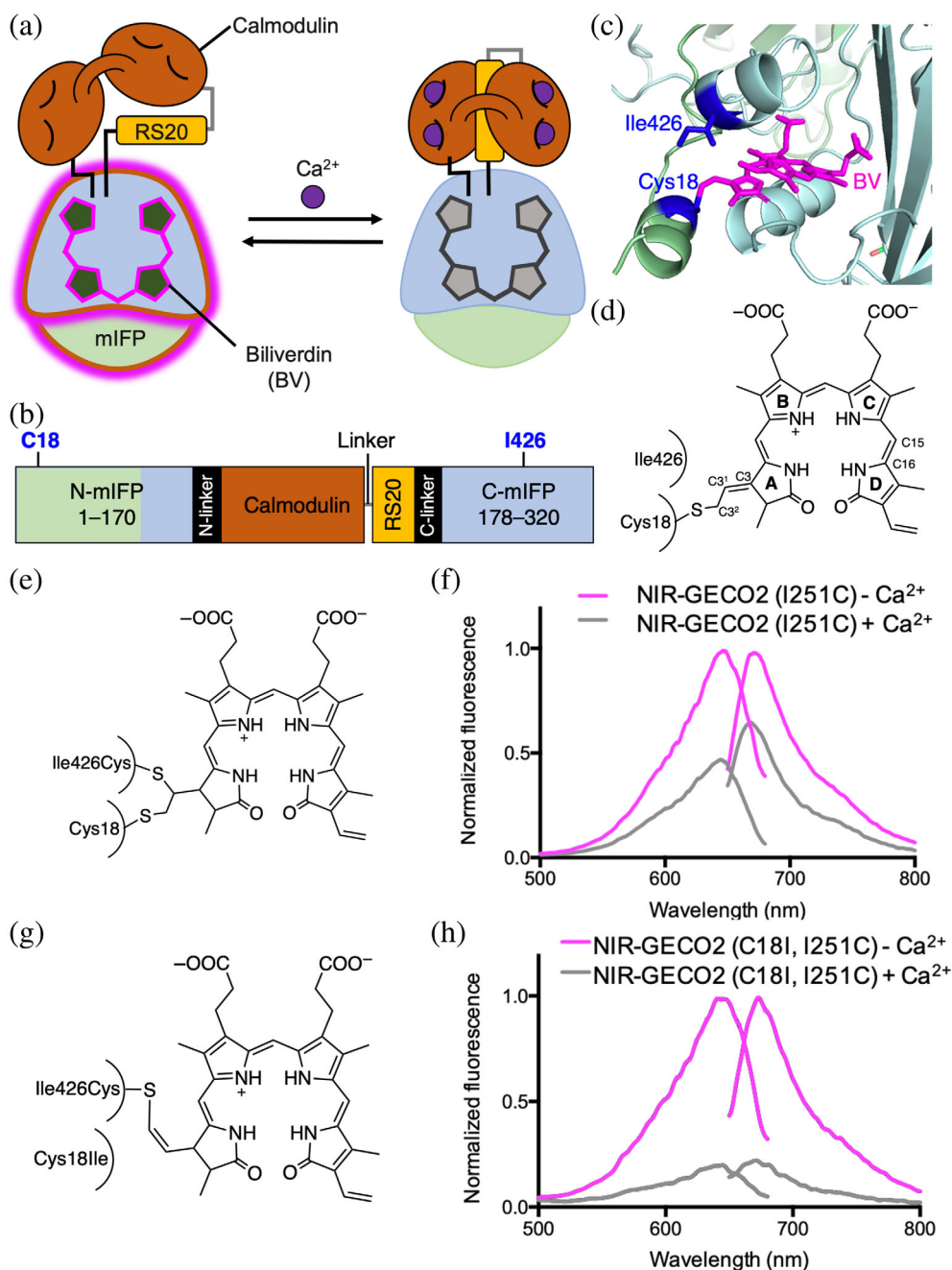


FIGURE 1 Engineering of a far-red Ca^{2+} biosensor prototype, iBB-GECO0.1. (a) Schematic representation of the mIFP-based NIR-GECO series GECIs and their inverse response to Ca^{2+} . The PAS (Per-ARNT-Sim) domain is colored light green and the BV-binding GAF (cGMP phosphodiesterase/adenylylase/FhlA transcriptional activator) domain is colored light blue. (b) Schematic representation of primary structure of the mIFP-based NIR-GECO series GECIs. (c) Modeled BV-binding site of mIFP based on a close mIFP homolog *DrBphP* (PDB 2O9B).³⁵ Cys18 and Ile426 (numbered as in NIR-GECO2) are colored in blue. (d) Schematic of the proposed chromophore structure of NIR-GECO2, with the characteristic linkage to BV shown.³⁶ The tautomer with double bond between C3 and C2 of the A-ring is also possible.^{11,37} (e) Schematic of the proposed chromophore structure in NIR-GECO2 Ile426Cys, by analogy to the “chromophore II” structure proposed by Baloban et al.¹¹ (f) Fluorescence excitation and emission spectra of NIR-GECO2 Ile426Cys in the presence (39 μM) and absence of Ca^{2+} . (g) Schematic of the proposed chromophore structure in NIR-GECO2 Cys18Ile/Ile426Cys, by analogy to the “chromophore I” structure proposed by Baloban et al.¹¹ We note that, mechanistically, it is not clear how such a linkage could form since it requires an oxidative hydride transfer step. (h) Fluorescence excitation and emission spectra of NIR-GECO2 Cys18Ile/Ile426Cys, also designated iBB-GECO0.1, in the presence (39 μM) and absence of Ca^{2+} . GECl, genetically encoded Ca^{2+} indicator.

2 | RESULTS

2.1 | Development of a far-red excitable Ca²⁺ biosensor prototype

In mIFP⁶ (and NIR-GECO2),⁵ the incorporation of BV involves the formation of a covalent thioether linkage between the cysteine at residue number 18 (equivalent to residue number 18 in NIR-GECO2) and the vinyl substituent on the A-ring of BV (Figure 1b–d).¹⁰ Mutation of Ile251 (equivalent to residue number 426 in NIR-GECO2) to cysteine results in formation of a second thioether linkage to the vinyl substituent on the A-ring of BV. The addition of the second thioether linkage is associated with blue-shifted excitation and emission due to the loss of one double bond from the conjugated system of the attached BV chromophore (Figure 1e). Indeed, we found that NIR-GECO2 Ile426Cys had a blue-shifted spectrum with excitation and emission maxima at 645 and 673 nm, respectively (Figure 1f). However, the Ile426Cys mutation also had the unwelcome effect of substantially decreasing the Ca²⁺ response ($\Delta F/F_{\min} \sim -0.5$) relative to NIR-GECO2 ($\Delta F/F_{\min} \sim -15$). We hypothesized that reduced sensitivity to Ca²⁺ might be associated with the double thioether linkage to the BV in NIR-GECO2 Ile426Cys. Accordingly, we introduced the Cys18Ile mutation to remove the original thioether bond formed between Cys18 and the A-ring of BV. The resulting variant retains the blue-shifted spectra (excitation maximum at 646 nm and emission maximum at 672 nm), possibly due to formation of the chromophore structure proposed by Balaban et al. (Figure 1g).¹¹ This variant has a better response to Ca²⁺ ($\Delta F/F_{\min} \sim -3.5$) than NIR-GECO2 Ile426Cys (Figure 1h). We designated the NIR-GECO2 Cys18Ile/Ile426Cys variant as iBB-GECO0.1, where iBB stands for iBlueberry.

2.2 | Development of a far-red excitable Ca²⁺ biosensor iBB-GECO1

To develop variants of iBB-GECO0.1 with improved brightness and greater Ca²⁺-dependent $\Delta F/F_{\min}$, we performed directed evolution (Figure S1a). In each round of directed evolution, we randomly mutated the whole gene by error-prone PCR, expressed the library in colonies of *Escherichia coli*, picked and cultured fluorescent clones, and spectroscopically characterized crude protein extracts.

After three rounds, we arrived at a variant named iBB-GECO0.4 which had 11 mutations relative to iBB-GECO0.1 and displayed $\Delta F/F_{\min}$ of -6.2 . One of these mutations was deletion of a glycine (G) residue in the

linker (GGGGS) between CaM and RS20. This result led us to explore the optimization of this linker length through systematic deletion of the glycine residues (Figure S1b). This linker optimization led to the identification of iBB-GECO0.5 in which a second G was deleted. Relative to iBB-GECO0.4, iBB-GECO0.5 was a modest improvement in terms of the higher Ca²⁺ response and higher Ca²⁺ affinity.

One additional round of evolution led to the identification of two promising variants that were designated as iBB-GECO1S and iBB-GECO0.6. iBB-GECO1S has a very high Ca²⁺ response ($\Delta F/F_{\min} \sim -35$). The other promising variant iBB-GECO0.6 has a comparable Ca²⁺ response ($\Delta F/F_{\min} \sim -7$) to iBB-GECO0.5, but its fluorescent intensity is much higher than iBB-GECO0.5 (crude protein extracts were 216% brighter). In an attempt to combine the beneficial mutations present in these two variants, we used the mixture of iBB-GECO1S and iBB-GECO0.6 as the gene template in the subsequent round of evolution. In this subsequent round, the most promising variant, designated iBB-GECO0.7, had a combination of mutations from iBB-GECO1S and iBB-GECO0.6, and had higher Ca²⁺ response ($\Delta F/F_{\min} = -9.3$) and brighter fluorescence intensity. Additional two rounds of evolution ultimately produced iBB-GECO1 with a higher Ca²⁺ response ($\Delta F/F_{\min} = -13$) (Table S1). iBB-GECO1 contains a total of 17 mutations relative to NIR-GECO2. Of the 17 mutations, two (C18I and I426C) are the initial mutations for spectral tuning, seven (M223L, D232N, T251A, Y271N, E276G, T282S, and M316I) are in CaM, five (S373Y, I378T, L391M, Q428L, and Q491P) are in the GAF domain of mIFP, one (F1a insertion after the start codon) is in the PAS domain of mIFP, and two (G321del and G322del) are the deletions in the linker between CaM and RS20 (Figures S2 and S3).

2.3 | In vitro characterization of iBB-GECO1

We undertook a detailed characterization of purified iBB-GECO1. iBB-GECO1 has two absorption peaks at 378 and 646 nm (Figure 2a). Ca²⁺ binding produces a change in absorption spectrum, with the peak at 646 nm decreasing and shifting to 659 nm, and the peak at 378 nm slightly increasing. Also, a far-red shoulder appears in the absorption spectrum near 740 nm. iBB-GECO1 shows excitation peak (Q-band) at 648 nm and emission peak at 668 nm (Figure 2b). The fluorescence emission maximum blue-shifts by 15 nm from 668 to 653 nm upon Ca²⁺ binding. In contrast to the Ca²⁺-dependent changes in the absorption profile, the profile

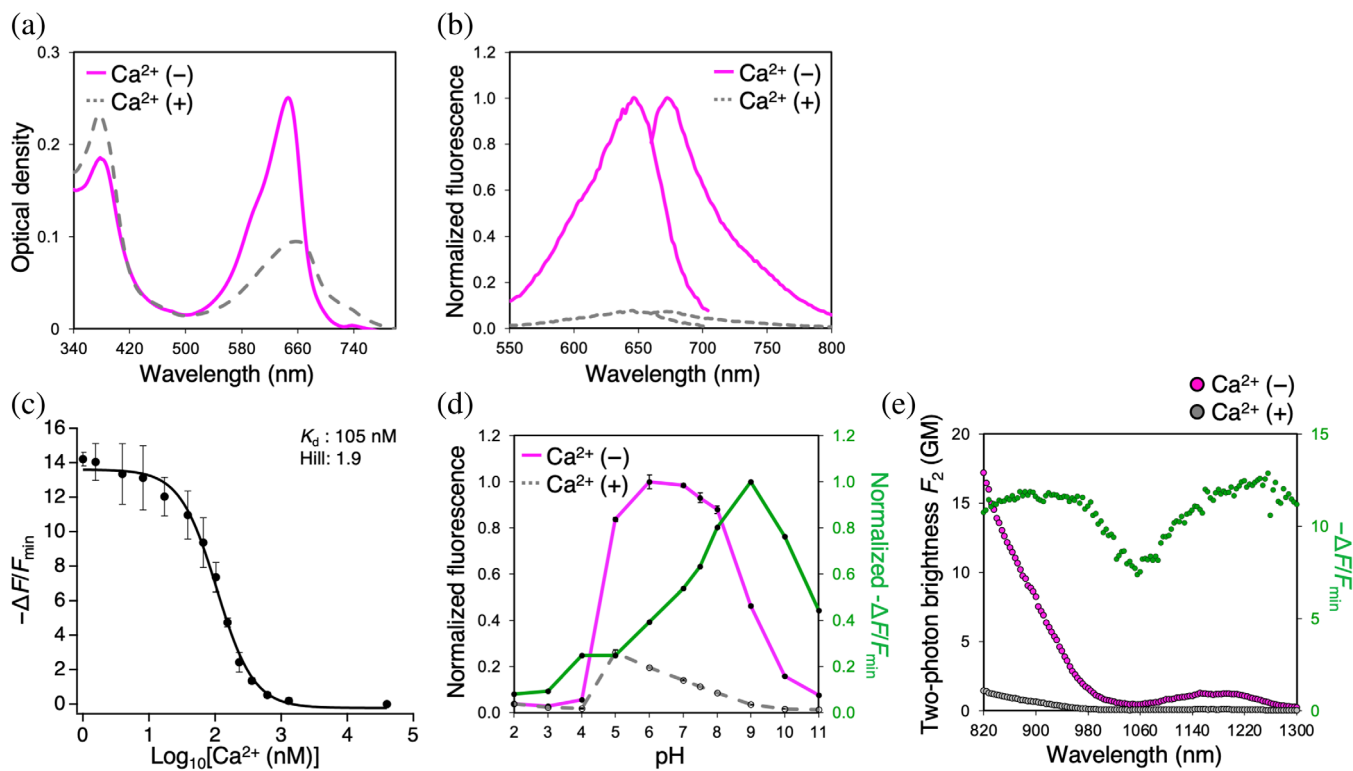


FIGURE 2 In vitro characterization of iBB-GECO1. (a) Absorbance spectra of iBB-GECO1 in the presence (39 μM) and absence of Ca^{2+} . (b) Fluorescence excitation (excitation from 550 to 705 nm and emission at 750 nm) and emission (excitation at 620 nm and emission from 660 to 800 nm) spectra of iBB-GECO1 in the presence (39 μM) and absence of Ca^{2+} . (c) $\Delta F/F_{\min}$ of iBB-GECO1 as a function of Ca^{2+} concentration (mean \pm SD, $n = 3$). (d) pH titration curves of iBB-GECO1 in the presence (39 μM) and absence of Ca^{2+} (mean \pm SD, $n = 3$). (e) Two-photon excitation spectra of iBB-GECO1 in the presence (39 μM) and absence of Ca^{2+} . $\Delta F/F_{\min}$ is represented in the green filled circles. GM, Goepfert-Mayer units.

of the fluorescence excitation spectrum in the Q-band region remains practically unchanged upon binding Ca^{2+} . In an attempt to elucidate the reason for the difference in the absorption and excitation spectra in the Ca^{2+} -bound state, we measured fluorescence lifetimes of both Ca^{2+} -free and bound states with excitation at 514 or 635 nm. The Gaussian distribution of the fluorescence lifetimes (with 514 nm excitation) becomes substantially broader in the Ca^{2+} -bound state (peak = 0.51 ns, width = 3.26 ns) relative to the Ca^{2+} -unbound state (peak = 1.18 ns, width = 0.78 ns) (Figure S4). Together with the observation of the far-red shoulder in the absorbance spectrum, these results suggest that iBB-GECO1 is in a single fluorescent state in the absence of Ca^{2+} , but in a variety of states (i.e., at least two 514 nm-excitable fluorescent states and one 740 nm-absorbing non-fluorescent state) when bound to Ca^{2+} .

The fluorescence signal of iBB-GECO1 exhibits an inverse response to Ca^{2+} binding ($\Delta F/F_{\min} = -13$) with an apparent dissociation constant (K_d) of 105 nM (Figure 2c). This relatively large $|\Delta F/F_{\min}|$ is presumably due to the combined contributions of changes in both extinction coefficient (70% decrease) and effective

quantum yield (73% decrease) (Table S1). The Hill coefficient of iBB-GECO1 is 1.9, indicating that iBB-GECO1 has higher cooperativity of Ca^{2+} binding than other members of the NIR-GECO series (Figure 2c, Table S1). In vitro characterization of iBB-GECO1 revealed the brightness of the Ca^{2+} unbound and bound state to be 90% and 7.2% of mIFP, respectively (Table S1). The fluorescence of iBB-GECO1 in the absence of Ca^{2+} has a bell-shaped pH dependence with $\text{p}K_a$ values of ~ 4.5 and ~ 9 (Figure 2d).

Under two-photon excitation, iBB-GECO1 has an intensimetric Ca^{2+} -induced fluorescence change ($\Delta F/F_{\min} = -11$ and -12 , at 820 and 1,200 nm, respectively) that is comparable to one-photon excitation (Figure 2e). Two-photon brightness per fluorophore (17 GM at 820 nm) of the Ca^{2+} -free iBB-GECO1 in the short-wavelength (Soret) region is much higher than that (2.4 GM at 900 nm) of NIR-GECO1 (Table S1).

iBB-GECO1S has an emission peak at 670 nm which is slightly red-shifted relative to iBB-GECO1 (Figure S5a). iBB-GECO1S undergoes larger Ca^{2+} -dependent changes in fluorescent intensity ($\Delta F/F_{\min} = -35$) with an apparent K_d of 70 nM and Hill coefficient of 1.8 (Figure S5b).

However, iBB-GECO1S is dimly fluorescent in live HeLa cells in the absence of exogenous BV (Figure S5c–f). Accordingly, we focused our further characterization efforts on iBB-GECO1.

2.4 | Characterization of iBB-GECO1 in live mammalian cells

When expressed in HeLa cells, iBB-GECO1 robustly decreased fluorescence intensity upon treatment with thapsigargin (TG) and CaCl_2 (Figure 3a). Administration of exogenous BV (12.5 μM) resulted in an approximately eightfold increase in the iBB-GECO1 baseline fluorescence (Figure 3b), indicating that $\sim 88\%$ of iBB-GECO1 was not bound to BV. The baseline fluorescence intensity of iBB-GECO1 is comparable to that of NIR-GECO2G in the both presence and absence of exogenous BV

(Figure 3b). iBB-GECO1 shows a higher fraction of bleed-through into the RFP channel (605/52 nm filter) than NIR-GECO2G, presumably due to its blue-shifted fluorescence (Figure 3c). Consistent with in vitro $\Delta F/F_{\min}$ and apparent K_d (Table S1), iBB-GECO1 has a larger $|\Delta F/F_{\min}|$ than NIR-GECO2G in mammalian cells (Figure 3d). Addition of exogenous BV (12.5 μM) has no significant effect on $\Delta F/F_{\min}$ of iBB-GECO1 and NIR-GECO2G, indicating that the fraction in the BV unbound state does not affect the Ca^{2+} -dependent response. To test photostability, we continuously illuminated iBB-GECO1-expressing HeLa cells using one-photon wide-field microscopy. The photobleaching rate of iBB-GECO1 is higher than that of mIFP and NIR-GECO2 (Figure 3e and Table S1). To characterize the performance of iBB-GECO1 in response to a more physiologically relevant change in the cytoplasmic Ca^{2+} concentration, HeLa cells were treated with histamine (Figure 3f). Upon treatment

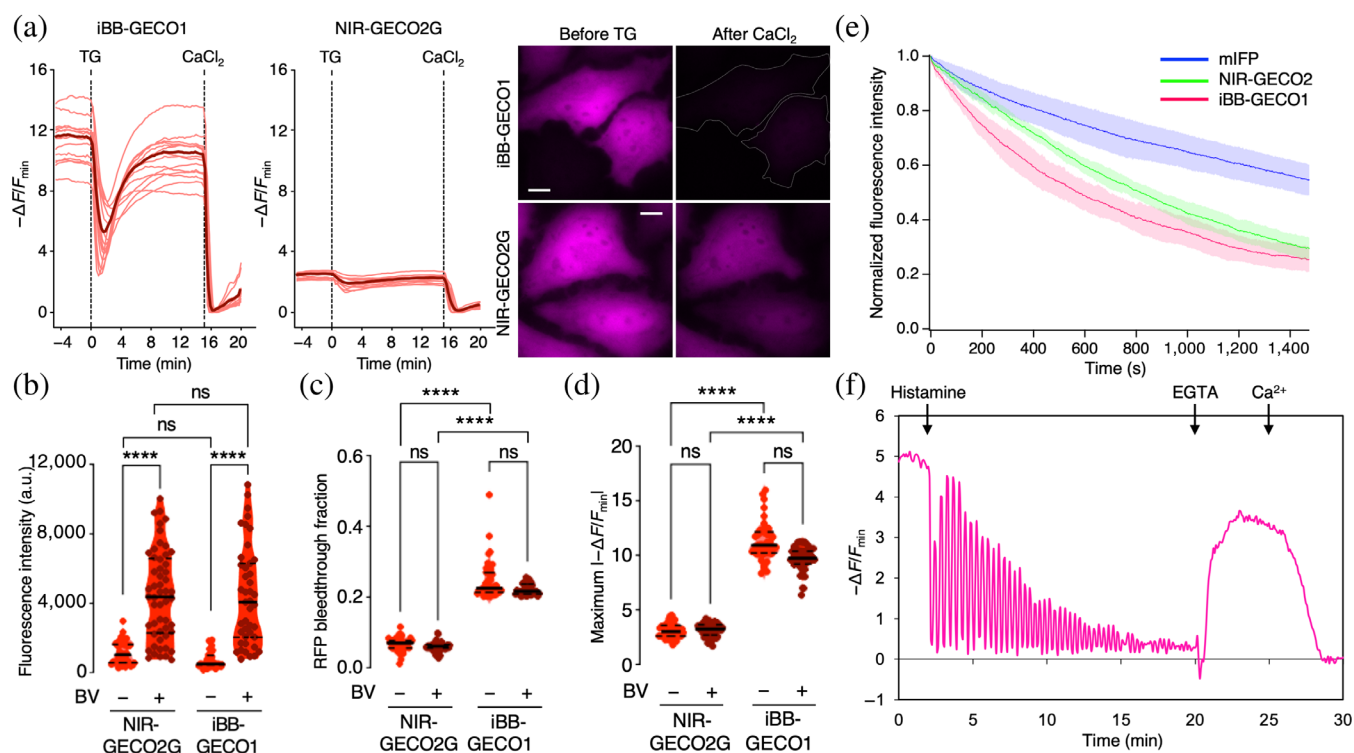


FIGURE 3 Characterization of iBB-GECO1 in live mammalian cells. (a) Fluorescence traces (left) from HeLa cells expressing iBB-GECO1 ($n = 15$ cells) or NIR-GECO2G ($n = 10$ cells) in response to bath application of TG and CaCl_2 , where $\Delta F/F_{\min} = (F_{\min} - F)/F_{\min}$ and F_{\min} represents the minimum fluorescence intensity for the whole trace. Thick and thin lines indicate mean and single-cell responses, respectively. Representative images (right) of iBB-GECO1 and NIR-GECO2G expressed in HeLa cells. Scale bars represent 10 μm . (b, c) Violin plots of (b) fluorescence brightness and (c) fraction of bleedthrough into RFP (605/52 nm) channel of NIR-GECO2G (–BV, $n = 41$ cells; +BV, $n = 53$ cells) and iBB-GECO1 (–BV, $n = 43$ cells; +BV, $n = 43$ cells) expressed in HeLa cells in the presence and absence of exogenous BV. n.s., not significant; **** $p < .0001$; Kruskal–Wallis test. (d) Violin plots of $-\Delta F/F_{\min}$ in HeLa cells expressing NIR-GECO2G (–BV, $n = 41$ cells; +BV, $n = 53$ cells) or iBB-GECO1 (–BV, $n = 43$ cells; +BV, $n = 43$ cells). n.s., not significant; **** $p < .0001$; Kruskal–Wallis test. (e) Photobleaching curves for iBB-GECO1 ($n = 11$ cells), mIFP ($n = 14$ cells), and NIR-GECO2 ($n = 12$ cells) expressed in HeLa cells. Solid lines represent mean value and shaded areas represent SD (f) Representative fluorescence trace of iBB-GECO1-expressing HeLa cell in response to bath application of histamine, EGTA, and Ca^{2+} .

with histamine, HeLa cells expressing iBB-GECO1 underwent oscillatory changes in fluorescence intensity. Treatment of the HeLa cells with EGTA and Ca^{2+} resulted in a maximum $\Delta F/F_{\min}$ of -2.6 ± 0.4 (mean \pm SD, $n = 5$ cells). Taken together, these results indicated that iBB-GECO1 is practically useful for imaging of intracellular Ca^{2+} concentration dynamics in mammalian cells.

2.5 | Two-photon imaging of iBB-GECO1 in live mammalian cells

Two-photon microscopy is widely used for Ca^{2+} imaging in the field of neuroscience. To investigate whether intracellular Ca^{2+} concentrations can be visualized using two-photon imaging of iBB-GECO1, we performed two-photon microscopy of HEK293T cells. The fluorescence intensity of iBB-GECO1 displayed oscillatory changes upon adenosine triphosphate (ATP) treatment (Figure 4a), demonstrating that iBB-GECO1 can enable the detection of changes in intracellular Ca^{2+} concentration with two-photon imaging. Dissociated primary

hippocampal neurons exhibited fluorescence spiking behavior (Figure 4b), suggesting that two-photon imaging of iBB-GECO1 can be used to visualize spontaneous neural activity.

In vitro characterization indicated that iBB-GECO1 shows a large Ca^{2+} -dependent fluorescence change by multiphoton excitation at 920 nm (Figure 2e). This wavelength is also optimal for excitation of GFP-based biosensors such as jRCaMP7, XCaMP-G, and XCaMP-Gf.^{12,13} To determine whether iBB-GECO1 and a GFP-based biosensor could be simultaneously excited at 920 nm, we independently expressed iBB-GECO1 and XCaMP-Gf in HEK293T cells and observed these cells in the same field of view (Figure 4c). ATP stimulation induced oscillations of fluorescence intensity of both iBB-GECO1 and XCaMP-Gf. Two-photon imaging of hippocampal primary neurons co-expressing iBB-GECO1 and XCaMP-Gf revealed fluorescent responses attributable to spontaneous neural activity (Figure 4d). Analysis of the fluorescent responses shows that iBB-GECO1 has slightly slower kinetics of Ca^{2+} response (Figure 4d). These results demonstrate that iBB-GECO1 can be simultaneously

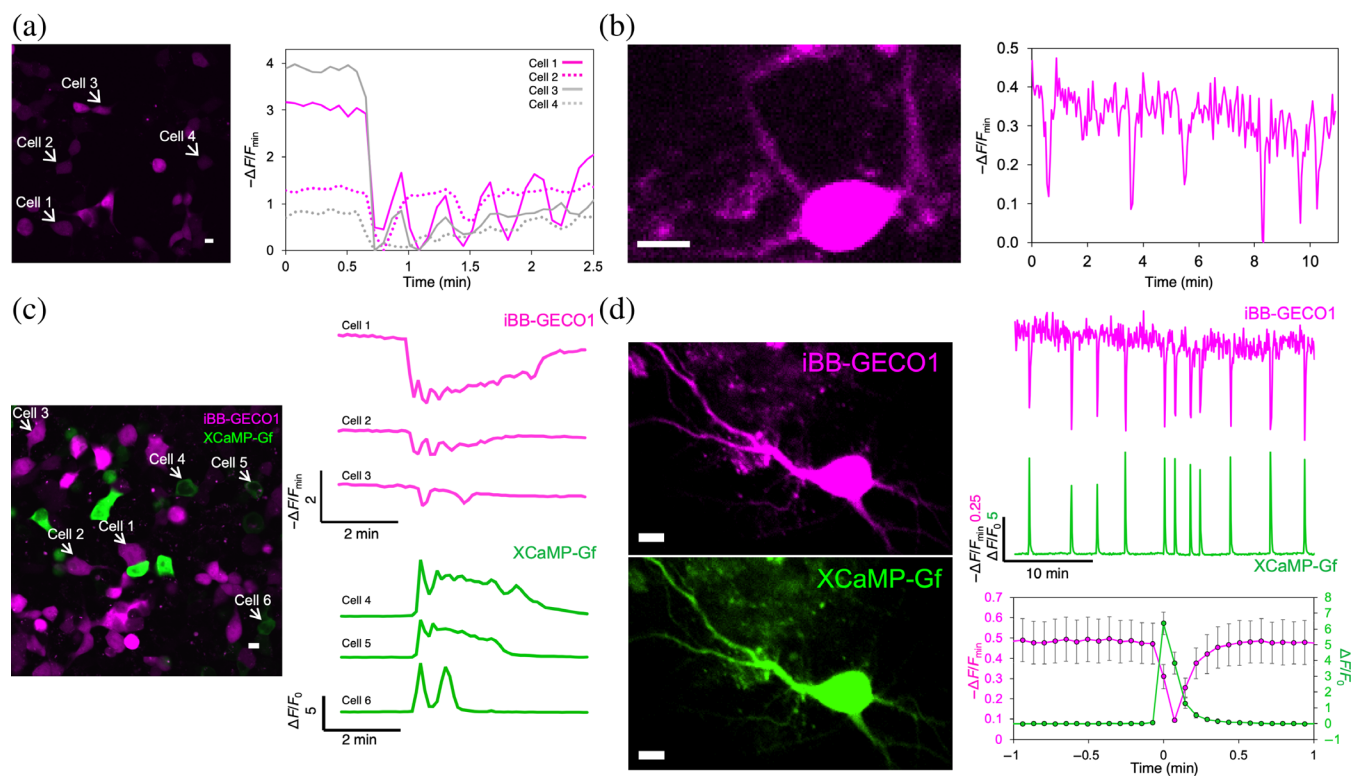


FIGURE 4 Two-photon imaging of iBB-GECO1 in live mammalian cells. (a) Two-photon (1,180 nm) imaging of ATP-induced Ca^{2+} oscillation in HEK293T cells expressing iBB-GECO1. (b) Two-photon (1,180 nm) imaging of spontaneous activity-dependent Ca^{2+} transients in hippocampal neurons expressing iBB-GECO1. (c) Two-photon (920 nm) dual-color imaging of ATP-induced Ca^{2+} oscillation in HEK293T cells expressing iBB-GECO1 or XCaMP-Gf. (d) Two-photon (920 nm) dual-color imaging of spontaneous activity-dependent Ca^{2+} transients in a hippocampal neuron co-expressing iBB-GECO1 and XCaMP-Gf. The right bottom graph represents a time trace of mean $-\Delta F/F_{\min}$ (iBB-GECO1) and $\Delta F/F_0$ (XCaMP-Gf) of within-cell-averaged transients from 8 neurons (mean \pm SEM). Scale bars, 10 μm .

visualized with a GFP-based biosensor in live mammalian cells using two-photon excitation at 920 nm.

In an attempt to evaluate the *in vivo* expression of iBB-GECO1, we induced expression of the genes of iBB-GECO1 and XCaMP-G in layer 2/3 (L2/3) of mouse cortex via *in utero* electroporation. Two-photon imaging of L2/3 cortical neurons supplemented with exogenous BV confirmed that iBB-GECO1 could be expressed *in vivo* (Figure S6a). Co-expression with XCaMP-G enabled us to visualize neuronal activity in a second spectral channel (Figure S6b). Image analysis based on correlation with XCaMP-G fluorescence revealed that iBB-GECO1 shows small but significant fluorescence changes in response to neural activity *in vivo* (Figure S6c).

2.6 | Multi-color live cell imaging of iBB-GECO1

Far-red excitable iBB-GECO1 could provide new color choice for multi-color imaging in combination with other fluorescent probes. To explore the applicability of iBB-

GECO1 for multi-color imaging, we performed four-color imaging using iBB-GECO1, the cyan- and yellow-FP-based protein kinase A (PKA) biosensor AKAR4,¹⁴ and the red-FP-based cAMP biosensor Pink Flamindo.¹⁵ Stimulation of MIN6 β -cells co-expressing these three biosensors with tetraethylammonium chloride (TEA) led to rapid and synchronous oscillations in Ca^{2+} , cAMP, and PKA activity (Figure 5a,b and Figure S7a). As another demonstration, we expressed five GECI color variants in co-cultured HEK293T cells: XCaMP-B, XCaMP-Gf, XCaMP-Y, XCaMP-R, and iBB-GECO1. The fluorescence signal from each GECI color variant was recorded during ATP-stimulation (Figure 5c and Figures S7b and S8). Overall, these results demonstrate that iBB-GECO1 is fully compatible with multi-color imaging in live mammalian cells.

3 | DISCUSSION

This study describes the development of a genetically encoded far-red fluorescent Ca^{2+} biosensor, designated

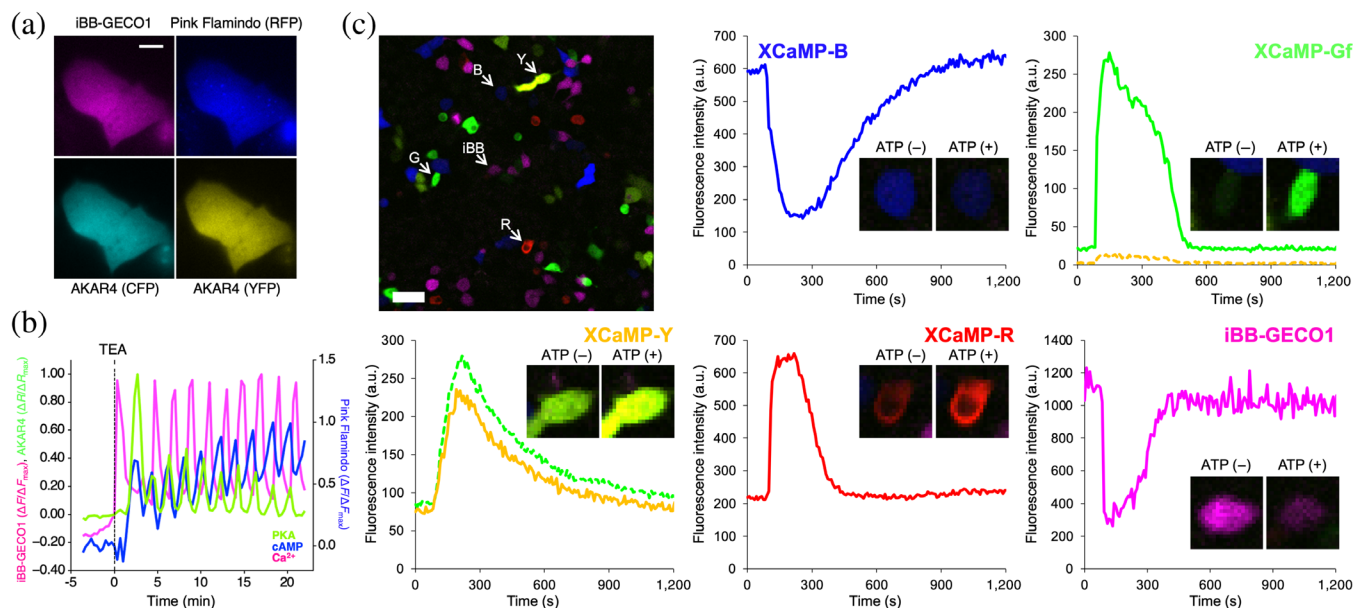


FIGURE 5 Multi-color imaging of iBB-GECO1 in live mammalian cells. (a) Representative fluorescence images of MIN6 β -cells coexpressing iBB-GECO1 (upper left), Pink Flamindo (upper right), and AKAR4 (bottom). Scale bar, 10 μm . (b) Simultaneous visualization of Ca^{2+} (iBB-GECO1; $\Delta F/\Delta F_{\text{max}}$, magenta line), cAMP (Pink Flamindo; $\Delta F/\Delta F_{\text{max}}$, blue line), and PKA (AKAR4; FRET emission ratio $\Delta R/\Delta R_{\text{max}}$, green line) in a MIN6 β -cell treated with 20 mM TEA at time zero. The emission ratio change ($R - R_0$) or fluorescence intensity change ($F - F_0$) was divided by the maximum ratio ($R_{\text{max}} - R_0$) or intensity ($F_{\text{max}} - F_0$) for Pink Flamindo and ($F_{\text{min}} - F_0$) for iBB-GECO1 change to obtain $\Delta R/\Delta R_{\text{max}}$ or $\Delta F/\Delta F_{\text{max}}$, with time zero defined as the time point immediately preceding drug addition. Traces for three additional representative cells are provided in Figure S7a. (c) Five-color Ca^{2+} imaging in co-cultured HEK293T cells expressing either XCaMP-B, XCaMP-Gf, XCaMP-Y, XCaMP-R, or iBB-GECO1. Blue, green, yellow, red, and magenta traces show fluorescence time courses for blue, green, yellow, red, or NIR channels for representative cells indicated by white arrows in the image, respectively. Identities of expressed GECIs were inferred from the relative intensities for the five channels. No significant spectral bleed through from other channels was observed in the blue, red, and NIR channels. There was substantial spectral bleed through between the green and yellow channels, as represented with the dashed lines. Insets in each fluorescence trace show cell images before and after ATP addition. Scale bar, 50 μm . Additional traces of cells expressing each biosensor are provided in Figure S7b. GECI, genetically encoded Ca^{2+} indicator.

iBB-GECO1, using the previously reported NIR-GECO2 GECI as a starting template. Rational mutagenesis of the BV binding pocket of NIR-GECO2 led to the identification of a biosensor prototype that has an excitation wavelength that is near-optimal for common ~ 630 – 640 nm laser lines on commercial microscopes. Extensive directed evolution of the prototype led to the far-red excitable Ca^{2+} biosensor, iBB-GECO1. iBB-GECO1 shows a high Ca^{2+} affinity (K_d of 105 nM) and a large inverse fluorescence response to Ca^{2+} ($\Delta F/F_{\min} = -13$ in vitro and -10 in HeLa cells). We have demonstrated that iBB-GECO1 can be used as a GECI under both one- and two-photon illumination microscopy. In addition, we have shown that iBB-GECO1 can enable 4- and 5-color imaging of Ca^{2+} dynamics in live mammalian cells.

iBB-GECO1 is our latest addition to a growing series of far-red and NIR excitable GECIs which includes FR-GECO1 and NIR-GECO1, 2, and 2G.^{4,5,16} The FR-GECO1 and NIR-GECO GECIs have excitation maxima at ~ 596 and ~ 678 nm, respectively (Table S1). These excitation peaks are too short and too long, respectively, to match well with commonly available helium-neon laser (633 nm) and semiconductor laser (~ 640 nm) lines. This wavelength mismatch could limit the achievable brightness on many microscope systems. GAF-CaMP3-sfGFP, developed by Subach and a coworker, has an excitation peak at 636 nm in Ca^{2+} -unbound state and 648 nm in Ca^{2+} -bound state.^{7,8} While this GECI has an excitation maxima that is better matched with the ~ 630 – 640 nm laser lines, it has a limited fluorescence response ($\Delta F/F_{\min} \sim 2$ in vitro and ~ 2.5 in HeLa cells). Furthermore, GAF-CaMP3-sfGFP requires cells to be supplemented with exogenous BV and it must be fused to sfGFP to give observable fluorescence in HeLa cells. iGECI, a FRET-based ratiometric GECI developed by Verkhusha and coworkers, also has an excitation peak near 640 nm, and provides a bright fluorescence without requiring a supplement of exogenous BV.⁹ However, the Ca^{2+} -dependent fluorescence change of iGECI is limited ($\Delta R/R \sim 0.6$).

As a new member of the series of far-red and NIR excitable GECIs, iBB-GECO1 has a unique combination of features that may make it particularly useful in certain contexts. In particular, iBB-GECO1 has an excitation peak at 648 nm in Ca^{2+} -unbound state and 646 nm in Ca^{2+} -bound state, both of which are highly optimal for commonly available laser lines. Furthermore, iBB-GECO1 displays a large magnitude of Ca^{2+} -dependent fluorescence change ($\Delta F/F_{\min} = -13$ in vitro, -10 in HeLa cells) without requiring a supplement of exogenous BV. For these reasons, iBB-GECO1 could potentially outperform previously reported far-red and NIR excitable GECIs when imaging cells or other thin tissues using

commonly available laser lines. The major disadvantage of iBB-GECO1 is that it is not practically useful for in vivo imaging in L2/3 of the mouse cortex due to its low brightness. Another disadvantage of iBB-GECO1, relative to NIR-GECO2, is that it is blue-shifted and therefore less suitable for deep tissue imaging, even if the brightness could be improved in future variants.

The in vitro photophysical characteristics of iBB-GECO1 provide some insights into a potential mechanism of fluorescence response to binding Ca^{2+} . In the Ca^{2+} -free state, the absorption and fluorescence excitation spectral profiles are practically identical in the Q-band region (Figure 2a,b), and the fluorescence decay is mono-exponential with similar lifetimes at both 514 and 635 nm excitation (Figure S4). Interestingly, the measurement of extinction coefficients of the Q-band based on the Strickler-Berg method, and another method that assumes a constant value for the Soret peak extinction coefficient, provided very similar values (Table S1). These results suggest a single conformation of the BV-protein complex that probably corresponds to a Pr (phytochrome red) form with the BV molecule in a 15Z isomeric state of pyrrole rings C and D (Figure 1d). The Pr form is not fluorescent in natural phytochromes because, upon photoexcitation, the C15 = C16 bond of BV isomerizes on a picosecond scale to 15E isomer that corresponds to the Pfr (phytochrome far-red) form. This Pfr form then relaxes back to Pr in dark. Presumably, the Pr-to-Pfr photoswitching in phytochrome-based NIR FPs and GECIs has been suppressed due to mutagenesis and engineering, allowing them to fluoresce in the Pr form.

Upon binding to Ca^{2+} , the main absorption peak (at 646 nm) of iBB-GECO1 decreases and changes its shape, and a far-red shoulder appears at ~ 740 nm (Figure 2a). In addition, the Gaussian distribution of the fluorescence lifetimes (with 514 nm excitation) becomes substantially broader upon Ca^{2+} binding (Figure S4). This supports the conclusion that the BV-protein system becomes more heterogeneous upon Ca^{2+} binding. Notably, the shoulder at ~ 740 nm is very similar to the absorption profile of the Pfr form^{17–19} (i.e., the 15E isomer with respect to the C15=C16 bond).²⁰ We propose that, due to conformational changes upon binding Ca^{2+} , a major fraction of the initial fluorescent Pr form transforms into a more red-shifted dark form and possibly one or more other species. This Ca^{2+} -dependent decrease in the concentration of the Pr form results in the intensometric decrease of fluorescence.

iBB-GECO1S is an intriguing variant of iBB-GECO1 that has a very high fluorescence response to Ca^{2+} ($\Delta F/F_{\min} = -28$) in vitro. Unfortunately, we found that iBB-GECO1S requires a supplement of exogenous BV to observe substantial fluorescence in mammalian cells

(Figure S5). In contrast, iBB-GECO1 provides adequate fluorescence without exogenous BV (Figure 3). These results suggest that a binding efficiency of BV to iBB-GECO1S is too low to enable efficient chromophore conjugation at the normal concentration of BV in cultured mammalian cells. iBB-GECO1S bears six mutations (N232D, T378I, Y396H, L428Q, S447F, and P491Q) relative to iBB-GECO1 (Figure S2). Of these six mutations, T378I, Y396H, and L428Q are located in the BV binding pocket (Figure S5g). NIR-GECO2 provides substantial fluorescence without exogenous BV,^{4,5} and the NIR-GECO2 template has the same residues of I378 and Q428 as iBB-GECO1S (Figure S2). Taken together, we suggest that the Y396H mutation could be primarily responsible for the low BV binding efficiency of iBB-GECO1S.

In contrast to the widespread application of β -barrel type FPs for in vivo imaging applications, the application of BV-binding FPs for in vivo imaging is still relatively limited. Almost certainly, the major factor limiting the widespread adoption of BV-binding FPs and GECIs is the limited availability of BV in mammalian cells. To improve the availability of BV in vivo, Kobachi and coworkers have developed a BV reductase knockout (KO) mouse line.²¹ Since the BV reductase is responsible for reducing BV to bilirubin, the BV reductase gene KO is expected to increase the concentration of BV in vivo. Indeed, expression of NIR-GECO1 in embryonic fibroblasts derived from the BV reductase KO mice showed a marked increase in fluorescence intensity compared to those derived from wild-type mice. As iBB-GECO1 shows some promise for in vivo imaging in a wild-type mouse (Figure S6), we anticipate that the use of BV reductase KO mice may enable improved in vivo multiplexed Ca^{2+} imaging. Furthermore, the substantial Ca^{2+} -dependent absorbance change and relatively low quantum yield of iBB-GECO1 (Table S1) suggests that this biosensor also has potential to serve as a Ca^{2+} reporter for photoacoustic (a.k.a. optoacoustic) imaging.²²

4 | MATERIALS AND METHODS

4.1 | General methods and materials

Taq DNA polymerase (New England Biolabs) was used for error-prone polymerase chain reaction (PCR). The QuikChange mutagenesis kit (Agilent Technologies) was used for site-directed mutagenesis. Restriction endonucleases, DNA ligation kits, and GeneJET miniprep kits were purchased from Thermo Fisher Scientific. Products of PCR and restriction digests were purified using agarose gel electrophoresis and the GeneJET gel extraction kit

(Thermo Fisher Scientific). DNA sequences were analyzed by DNA sequence service of Fasmac Co., Ltd. Fluorescence excitation and emission spectra were recorded on Safire2 and Spark plate readers (Tecan).

4.2 | Engineering of iBB-GECO1

The gene encoding NIR-GECO2 in pDuet2 vector that includes the gene of cyanobacteria *Synechocystis*-derived heme oxygenase-1 (HO-1) was used as the starting template in this study. Site-directed mutagenesis of NIR-GECO2 was performed to produce iBB-GECO0.1. The gene encoding iBB-GECO0.1 was randomly mutated by error prone PCR. The condition for error-prone PCR was optimized to satisfy 1–2 mutations per 1,000 base pairs by varying the concentration of manganese ion (Mn^{2+}) in the PCR reaction. Gene fragments encoding the iBB-GECO library were then ligated with pDuet2 via restriction sites of XhoI and HindIII. The ligation product was used to transform *E. coli* strain DH10B (Thermo Fisher Scientific) and plated on Petri dishes containing LB agar. We picked the brightest 5–10% colonies of approximately 10^5 colonies in each round and cultured each colony in 1 ml of LB medium supplemented with $100 \mu\text{g ml}^{-1}$ ampicillin in 96-deep well plates. After incubation of the plates at 37°C for 20 hr followed by 24 hr at room temperature, proteins were extracted using B-PER bacterial protein extraction reagent (Thermo Fisher Scientific) and tested for fluorescence brightness and Ca^{2+} -dependent fluorescence response. A variant with the highest fluorescence response (F/F_{\min} , where F and F_{\min} are fluorescence intensity in the absence and presence [$39 \mu\text{M}$] of Ca^{2+} , respectively) and the highest fluorescence intensity (F) was identified as a promising variant in each round. DNA sequence of the best iBB-GECO variant was analyzed and then the DNA was served as template for the next round. When there were several promising variants, we combined DNA encoding these variants and used their mixture as the template for the next round of directed evolution.

4.3 | iBB-GECO1 expression vectors

For expression of iBB-GECO1 in bacteria and HeLa cells, the original pDuet2 vector was used. For expression in MIN6 β -cells, we cloned the gene of iBB-GECO1 into pCDNA3. For expression in HEK293T cells, dissociated neurons, and in vivo, the gene of iBB-GECO1 was inserted into vectors with CAG promoter and CaMKII promoter to develop pCAG-iBB-GECO1 and pCaMKII-iBB-GECO1, respectively.

4.4 | Protein purification and in vitro characterization

The gene encoding iBB-GECO1, with a poly-histidine tag on the C-terminus, was expressed from the pDuet2 vector in *E. coli* strain DH10B. The bacteria were lysed with a cell disruptor (Branson) and then centrifuged at 15,000g for 30 min. Extracted protein contained in the supernatant was purified by Ni-NTA affinity chromatography (Agarose Bead Technologies). The eluted sample was further concentrated and desalted with an Amicon Ultra-15 Centrifugal Filter Device (Merck).

To quantitatively compare absorption spectra of iBB-GECO1 in Ca^{2+} -free and Ca^{2+} -bound states, we prepared the sample with the same concentrations of the iBB-GECO1 protein in Ca^{2+} (–) buffer (30 mM 3-morpholinopropane-1-sulfonic acid (MOPS), 10 mM ethylene glycol-bis (β -aminoethyl ether)-*N,N,N',N'*-tetraacetic acid (EGTA), 100 mM KCl, pH 7.2) and Ca^{2+} (+) buffer (30 mM MOPS, 10 mM EGTA, 100 mM KCl, 10 mM CaCl_2 , pH 7.2) and measured their absorption spectra with a Lambda950 spectrophotometer (Perkin Elmer) in 1-cm glass cuvettes.

To perform pH titrations, 10 μl of protein solutions were diluted into 90 μl of buffers (pH from 2 to 11) containing 30 mM trisodium citrate, 30 mM sodium borate, 30 mM MOPS, 100 mM KCl, 10 mM EGTA, and either no CaCl_2 or 10 mM CaCl_2 . Fluorescence intensities as a function of pH were then fitted by a sigmoidal binding function to determine the $\text{p}K_a$.

For Ca^{2+} titration, the purified protein solution was diluted into a series of buffers, which were prepared by mixing Ca^{2+} (+) buffer and Ca^{2+} (–) buffer with final free Ca^{2+} concentration in a range from 0 to 36 μM . Fluorescence intensities were plotted against Ca^{2+} concentrations and fitted by a sigmoidal binding function to determine the Hill coefficient and apparent K_d .

Fluorescence quantum yields (QYs) were measured with an integrating sphere fluorometer (Quantaaurus-QY, Hamamatsu) using 1-cm quartz cuvettes at a set of excitation wavelengths varying from 560 to 600 nm with the step of 5 nm. QYs are presented as an average of these data. The peak optical density (OD) of the samples was <0.1. The reference (buffer only) measurements were done in the same cuvette as was used for the sample.

To determine extinction coefficients (ECs), we used two different methods. The first method compares OD at the Q peak to the OD at the Soret peak and assumes that an extinction of the latter is $39.9 \text{ mM}^{-1} \text{ cm}^{-1}$.²³ For a one-component solution, this method provides an actual EC at the Q-peak of the component. If a mixture of different conformers of BV is present, this method gives an effective EC of a particular component i : $\varepsilon_i^* = \rho_i \varepsilon_i$, where

ρ_i is a fractional concentration of this component ($\sum_i \rho_i = 1$) and ε_i is its EC. Here, it is also assumed that each conformer has the same EC and the same spectral position of the Soret peak. In the second method, we do not make any assumptions about the extinction of the Soret peak. This method uses the Strickler-Berg formula²⁴ relating fluorescence lifetime and QY to the integral over absorption band, expressed in EC values. This pure photophysical approach was described in detail previously.²⁵ It works only for mono-component systems without any geometry change of the fluorophore in the excited state.

Fluorescence lifetimes were measured with a Digital Frequency Domain system ChronosDFD (ISS), as previously described.²⁶ Fluorescence was excited with a 514-nm laser diode (ISS) or 635-nm laser diode (ISS). Rose Bengal (Sigma–Aldrich) in methanol with $\tau = 0.55 \text{ ns}$ ²⁶ and LDS798 in ethanol with $\tau = 0.15 \text{ ns}$ ²⁷ were used as reference standards to obtain the instrumental response function at 514- and 635-nm excitation wavelengths, respectively. Fluorescence was collected through a combination of 520LP and 561LP filters for 514-nm excitation and through 695LP and 705/100 filters for 635-nm excitation. To analyze the fluorescence lifetime data, we used a continuous Gaussian distribution of decay lifetimes with the center $\langle \tau \rangle$ and dispersion w (Vinci 3 software, ISS).

To collect relative two-photon excitation spectra, we used the methods and protocols described elsewhere.²⁸ To obtain the two-photon molecular brightness spectrum $F_2(\lambda)$ in the Goepfert–Mayer (GM) units, we scaled the relatively-corrected excitation spectra to the numbers of molecular brightness $F_2 = \sum_i \sigma_{2,i} \rho_i \varphi_i$, where $\sigma_{2,i}$ and φ_i are the two-photon absorption cross section and fluorescence QY of component i , respectively, measured at a selected wavelength. The F_2 values of iBB-GECO1 in the Ca^{2+} -free and Ca^{2+} -bound states were measured as described previously,¹⁶ relatively to Rhodamine 6G in ethanol ($\sigma_2[1,060 \text{ nm}] = 10 \text{ GM}$),²⁸ or Rhodamine B in alkaline ethanol ($\sigma_2[1,064 \text{ nm}] = 13.3 \text{ GM}$),¹⁶ using a combination of 770/SP and 561LP filters (Semrock). The results obtained with these two references were very close and the average values were used to scale the two-photon excitation spectra.

4.5 | Imaging of iBB-GECO1 in HeLa and HEK293T cells

HeLa cells were maintained in Dulbecco's modified Eagle medium (DMEM; Nakalai Tesque) containing 4.5 g L^{-1} glucose, supplemented with 10% (v/v) fetal bovine serum (FBS; Sigma–Aldrich) and 1% (v/v) penicillin–

streptomycin (Nakalai Tesque) at 37°C and 5% CO₂. Cells were seeded in 35-mm glass-bottom cell-culture dishes (Iwaki) and transiently transfected with 2 µg of the constructed plasmid using polyethylenimine (Polysciences). Transfected cells were imaged 48 hr after transfection using an IX83 wide-field fluorescence microscopy (Olympus) equipped with a pE-300 LED light source (CoolLED), a 40× objective lens (numerical aperture [NA] = 1.3; oil), an ImageEM X2 electron-multiplying charge-coupled device (EM-CCD) camera (Hamamatsu), Cellsens software (Olympus) and a STR stage incubator (Tokai Hit). Immediately prior to imaging, cells were washed twice with Hank's balanced salt solution (HBSS) and then 1 ml of 10 mM HEPES buffered HBSS (HHBSS) was added. The filter set used in live cell imaging had the following specification. iBB-GECO1 (histamine-inducing Ca²⁺ oscillation): excitation 615/20 nm, dichroic mirror 640-nm dclp, and emission 670/50 nm; iBB-GECO1 (photostability) and NIR-GECO2: excitation 655/40 nm, dichroic mirror 685-nm dclp, and emission 716/40 nm. Fluorescence images were analyzed with ImageJ software (National Institutes of Health).²⁹

For quantitative comparison of the performance of iBB-GECO1 and NIR-GECO2G, HeLa cells were cultured in DMEM (Gibco) containing 1 g L⁻¹ glucose and supplemented with 10% (v/v) FBS (Sigma), 1% (v/v) penicillin-streptomycin (Sigma-Aldrich) and maintained in a humidified incubator at 37°C with a 5% CO₂ atmosphere. For imaging, cells were plated onto sterile, 35-mm glass-bottomed dishes (CellVis) and grown to 50–70% confluence. Cells were transfected with 0.5 µg of iBB-GECO1 or NIR-GECO2G using Lipofectamine 2000 (Invitrogen). Excess transfection reagent was removed after 2 hr by exchanging the culture medium with fresh DMEM. At 24 hr after transfection, cells were washed twice with HBSS (Gibco) and subsequently imaged in HBSS. For BV pretreatment, cells were placed in HBSS supplemented with 12.5 µM BV (Cayman Chemical) and incubated for 1 hr at 37°C in a CO₂-free incubator. HeLa cells were then imaged at 37°C on a Zeiss AxioObserver Z1 inverted epifluorescence microscope (Carl Zeiss) equipped with a 40×/1.3 NA objective and a Photometrics Evolve 512 EMCCD (electron-multiplying charge-coupled device) camera (Photometrics) controlled by META-FLUOR 7.7 software (Molecular Devices). iBB-GECO1 or NIR-GECO2G intensity was imaged using a 640DF30 excitation filter, a 700DF75 emission filter, and a T660LPXR dichroic mirror. For bleedthrough measurements, RFP intensity was imaged using a 555DF25 excitation filter, a ZT568RDC dichroic mirror, and a 650DF100 emission filter. All filter sets were alternated by a Lambda 10-2 filter-changer (Sutter Instruments). Images were acquired every 15 s with exposure time of 500 ms and

EM gain of 10. Fluorescence images were corrected by background subtraction, and responses were plotted as $-\Delta F/F_{\min} = -(F_{\min} - F)/F_{\min}$, where F_{\min} is the minimum fluorescence intensity recorded after Ca²⁺ stimulation. The fraction of bleedthrough (C) into the RFP channel was calculated as $C = I_{\text{RFP}}/I_{\text{mIFP}}$, where I_{RFP} and I_{mIFP} are the fluorescence intensities recorded at 650/100 nm and 700/75 nm emission, respectively, for iBB-GECO1- or NIR-GECO2G-expressing HeLa cells.

HEK293T cells (CRL11268, ATCC) were cultured in DMEM (D5796, Sigma-Aldrich) supplemented with FBS and Penicillin-Streptomycin (15070-063, Thermo Fisher) at 37°C and 5% CO₂ in a humidified atmosphere. For five-color imaging, the genes encoding pCAG-iBB-GECO1, pCAG-XCaMP-B, pCAG-XCaMP-Gf, pCAG-XCaMP-Y, and pCAG-XCaMP-R were independently transfected using X-treme GENE 9 (6365809001, Merck Millipore) into HEK293T cells in different wells so that the cells in each well express only one of the five indicators. The day before imaging, these cells were treated with trypsin and replated on the same glass bottom dish (P35G-0-10-C, MatTek) so that cells expressing one of the five indicators are in the same field of view. Five-color live-cell imaging was performed in Tyrode's solution (129 mM NaCl, 5 mM KCl, 30 mM glucose, 25 mM HEPES-NaOH, pH 7.4, 2 mM CaCl₂, 1 mM MgCl₂; osmolality was adjusted to that of the conditioned culture medium using sucrose) using FV3000 confocal microscopy (Olympus) equipped with 30×/1.05 NA silicone-immersion objective (UPLSAPO30XS, Olympus), five laser lines reflected by BS10/90 (Olympus), and two detectors separated by dichroic mirror SDM400-580 (Olympus). The HEK293T cells were treated with 1/9 volume of 1 mM ATP (01072-11, Nacalai tesque) dissolved in Tyrode's solution to be the final concentration of 100 µM.

For two-photon imaging, HEK293T cells were imaged using an Olympus FVMPE-RS microscope equipped with a 25×/1.05 NA water-immersion objective (XLPLN25XWMP2). iBB-GECO1 was excited by a 1180 nm laser (InSight X3 Dual, Spectra-Physics) and imaged by non-descanned detector using a 32BA660-750 emission filter (Olympus) and a SDM570 dichroic mirror (Olympus). For dual-color two-photon imaging, iBB-GECO1 and XCaMP-Gf were simultaneously excited by a 920 nm laser and their fluorescence signals were imaged by two non-descanned detectors using a SDM570 dichroic mirror (Olympus) with a 32BA660-750 emission filter (Olympus) for iBB-GECO1 and 32BS495-540 emission filter (Olympus) for XCaMP-Gf. Fluorescence images were corrected by background subtraction, and the fluorescence response of iBB-GECO1 was plotted as $-\Delta F/F_{\min} = -(F_{\min} - F)/F_{\min}$, where F_{\min} is the minimum

fluorescence intensity for the whole traces. Fluorescence response of XCaMP-Gf was plotted as $\Delta F/F_0 = (F - F_0)/F_0$, where F_0 is the mean of fluorescence intensity before ATP bath application. The five probes in the same field of view were discriminated by relative fluorescence intensities for the five channels, referring standard samples in which cells expressing one of the five probes.

4.6 | Multiplexed live-cell imaging with iBB-GECO1 in MIN6 β -cells

MIN6 pancreatic β -cells were cultured in DMEM (Gibco) containing 4.5 g L⁻¹ glucose, supplemented with 10% (v/v) FBS (Sigma), 1% (v/v) penicillin-streptomycin (Sigma-Aldrich), and 50 μ M β -mercaptoethanol (Sigma-Aldrich), and were maintained at 37°C with a 5% CO₂ atmosphere. Cells were plated onto 35-mm glass-bottom dishes (CellVis), grown to 40–60% confluence and then transfected with 0.5 μ g each of plasmids encoding AKAR4 (PMID 20838685), Pink Flamindo (PMID 28779099) and iBB-GECO1 using Lipofectamine 2000 (Invitrogen). After 48 hr, cells were washed twice with HBSS (Gibco) and imaged in HBSS at 37°C using a Zeiss AxioObserver Z1 inverted epifluorescence microscope (Carl Zeiss) equipped with a 40 \times /1.3-NA objective, a Lambda 10–2 filter-changer (Sutter Instruments) and a Photometrics Evolve 512 EM-CCD camera (Photometrics) controlled by METAFLUOR v.7.7 software (Molecular Devices). Filters for cyan/yellow emission ratio imaging were a 420DF20 excitation filter, a 450DRLP dichroic mirror, and 475DF40 (CFP) and 535DF25 (YFP) emission filters. Filters for RFP were a 555DF25 excitation filter, a ZT568RDC dichroic mirror, and a 650DF100 emission filter. Filters for iBB-GECO1 were a 640DF30 excitation filter, a 700DF75 emission filter, and a T660LPXR dichroic mirror. All filter sets were alternated by a Lambda 10-2 filter-changer (Sutter Instruments). Images were acquired every 20 s with exposure time of 500 ms and EM gain of 10 (AKAR4) or 50 (Pink Flamindo and iBB-GECO1). Fluorescence intensities were corrected by background subtraction. Corrected RFP (650/100 emission) intensities were calculated as $I_{RFP}' = I_{RFP} - (C \times I_{mIFP})$, where I_{RFP}' and I_{RFP} are the corrected and uncorrected RFP intensities, respectively, I_{mIFP} is the mIFP (iBB-GECO1) intensity, and C is the correction factor calculated above. The emission ratio change ($R - R_0$) or fluorescence intensity change ($F - F_0$) was divided by the maximum ratio ($R_{max} - R_0$) or intensity ($F_{max} - F_0$) for Pink Flamindo and ($F_{min} - F_0$) for iBB-GECO1 change to obtain $\Delta R/\Delta R_{max}$ or $\Delta F/\Delta F_{max}$, with time zero defined as the time point immediately preceding drug

addition. Graphs were plotted using GraphPad Prism 9 (GraphPad Software).

4.7 | Imaging of iBB-GECO1 in dissociated neuron cultures

For the preparation of dissociated hippocampal neuron culture, postnatal day 0 or 1 Sprague–Dawley rats (SLC, Japan) were used as previously described.³⁰ Briefly, dissected hippocampal tissue was digested with Trypsin for 5 min at room temperature and washed with HBSS buffer (H4891, Sigma–Aldrich) containing 20% FBS once and with HBSS buffer three times. Digested tissue was gently dissociated with siliconized Pasteur pipettes, and dissociated neurons were plated at a density of 5×10^4 – 6×10^4 per glass bottom dish coated with Matrigel (CB-40234, Corning). Neurons were cultured in medium containing MEM (51200-038, Thermo Fisher), 0.5% D-glucose (16806-25, Nacalai Tesque), 0.02% sodium hydrogen carbonate (31213-15, Nacalai Tesque), 0.01% transferrin (820572, Merck Millipore), 2 mM Glutamax (35050-061, Thermo Fisher), 0.0025% insulin (I5500, Sigma–Aldrich), 2% B27 supplement (17504-044, Gibco), and 10% heat-inactivated FBS at 37°C and 5% CO₂ in a humidified atmosphere. Two days after the plating (2 days in vitro, DIV), culture medium containing MEM, 0.5% D-glucose, 0.02% sodium hydrogen carbonate, 0.01% transferrin, 0.5 mM Glutamax, 0.0025% insulin, 2% B27 supplement, 5% heat-inactivated FBS, and 0.008 mM AraC (C6645, Sigma–Aldrich) was added. AraC-free culture medium containing 5% FBS was further added on DIV 5 and one third of the culture medium was exchanged by fresh medium containing 5% FBS on DIV 8.

On DIV 9, pCAG-iBB-GECO1 and pCAG-XCaMP-Gf or pCaMKII-iBB-GECO1 and pCaMKII-XCaMP-Gf were transfected using Lipofectamine 2000 (11668019, Thermo Fisher). After 4–6 days, neurons were then imaged in Tyrode's solution using Olympus FVMPE-RS under the same optical settings as the two-photon imaging of HEK293T cells. The same method used for HEK293T cells as described above. Fluorescence images were analyzed by ROI manager module of ImageJ software. After background subtraction, and the fluorescence response of iBB-GECO1 was plotted as $-\Delta F/F_{min} = -(F_{min} - F)/F_{min}$, where F_{min} is the minimum fluorescence intensity for the whole traces and the fluorescence response of XCaMP-Gf was plotted as $\Delta F/F_0 = (F - F_0)/F_0$, where F_0 is the mean of the bottom 20% fluorescence intensity for the whole traces. To calculate the population average of spontaneous neural activity for dual-color imaging of iBB-GECO1 and XCaMP-Gf, the onsets of spontaneous fluorescent rising events were detected by XCaMP-Gf

fluorescence change. A neuronal activity event was defined as the time when the $\Delta F/F_0$ of XCaMP-Gf exceeded both the mean + 4 SDs and twice the mean of the previous 15 frames, and when there was no such events in the previous 8 frames. Events were subjected to visual inspection and excluded from the further analysis if multiple transients were closely observed. For each cell, 4–9 events were time-locked to the onset and averaged to calculate their transient. Finally, the mean and standard error of the mean of 9 cells are shown in the population average trace.

4.8 | Surgery of mice for in vivo imaging of iBB-GECO1

In utero electroporation was fundamentally performed as previously reported.¹² Briefly, embryonic day (E) 15 timed-pregnant ICR mice (Japan SLC) were anesthetized with three types of mixed anesthetic agents—Medetomidine/Midazolam/Butorphanol (MMB)—at a dose of 10 ml kg⁻¹ body weight. Approximately 2.0 μ l of purified plasmid solution containing Fast Green (Wako Pure Chemical Industries, Ltd.) as a marker was injected into the lateral ventricle of mouse embryos. Seven electrical pulses of 45 V (50 ms on, 950 ms off at 1 Hz) were delivered by an electroporator (BTX), targeting the barrel cortex. Two plasmids, pCAG-iBB-GECO1 (4.0 μ g μ l⁻¹) and pCAG-XCaMP-G (4.0 μ g μ l⁻¹) were used at a 20:1 ratio.

Imaging surgery was performed by a previously described method with slight modifications.^{31,32} Briefly, the mice (24–30 days) were anesthetized with MMB (10 ml kg⁻¹ body weight), then placed in head holders (KOPF). After removing the scalp and disinfection of the skull with a 70% (vol/vol) ethanol solution, the skull was drilled as small a hole as possible with a dental drill. BV hydrochloride (Sigma) was dissolved in a 4% DMSO solution and then diluted with normal mouse ringer (135 mM NaCl, 5.4 mM KCl, 1 mM MgCl₂, 1.8 mM CaCl₂, and 5 mM HEPES, adjusted to pH 7.2) to a concentration of 1 mM. One microliters of the BV solution was air-pressure injected through a glass pipette with a tip diameter of 50 μ m. The injection site was the central location where the craniotomy was to be performed in the barrel region, and the injection depth was 200 μ m below the pia mater. The injection was completed within 30 min. After placing the mouse on the head holders (Narishige), a craniotomy with a diameter of 3.5 mm was performed centered on the injection site. The craniotomy was covered with a window glass consisting of two different-sized micro cover-glasses (3.5 and 4.5 mm in diameter, Matsunami Glass Ind.) that were adhered to using a UV-curing resin. The cover-glasses and a custom-

made head plate were cemented to the skull with dental cement (Sun Medical). During surgery, the body temperature of the mice was monitored with a thermometer and maintained with a hand warmer. Their eyes were coated with white petroleum (Maruishi Pharmaceutical Co. Ltd.). The replacement of the skull with the cover glasses was completed within 90–120 min.

4.9 | In vivo imaging of iBB-GECO1

Immediately after the surgery, in vivo imaging of L2/3 cortical neurons in the anesthetized mice was performed using a two-photon microscope (FVMPE-RS, Olympus) equipped with a 25 \times /1.05 NA water-immersion objective (XLPLN25XWMP2, Olympus). The head plate cemented to mice was firmly screwed to a custom-made apparatus, and it was moved under the microscope. Neurons co-expressing iBB-GECO1 and XCaMP-G were excited at 920 nm with a Ti:sapphire laser (InSight X3 Dual, Spectra-Physics), and their fluorescence signals were separated by a 570 nm dichroic mirror and collected by two photomultiplier tubes through emission filters at 660–750 nm for iBB-GECO1 and 495–540 nm for XCaMP-G. A field of view of 255 \times 255 μ m² was scanned with resonant galvanometric scanners. Images were acquired with a total pixel count of 512 \times 512, with 4-times line averaging, at approximately 7.5 frames per second, and in 10-bits.

4.10 | Analysis of in vivo imaging data

Motions of the imaging data for iBB-GECO1 were corrected using NoRMCorre,³³ and the correction values were applied to the imaging data for XCaMP-G. Neurons were detected from a motion-corrected 500-frame average image of iBB-GECO1. Regions of interests (ROIs) were manually drawn using “ROI Manager” provided in ImageJ. $\Delta F/F_0$ was calculated as $(F(t) - F_0(t))/F_0(t)$, where t is time and F_0 is the baseline fluorescence. The F_0 was estimated considering fluorescence photobleaching. First, we separated t into two periods: periods t_{on} when neurons were active and t_{off} when neurons were inactive, referring to the fluorescence change of XCaMP-G. Then, we fitted an exponential function to the $F(t_{\text{off}})$ to obtain $F_0(t)$ for XCaMP-G and iBB-GECO1, respectively.

For in vivo imaging data analysis, we focused on $\Delta F/F_0$ induced by spontaneous neural activity. The following procedure identified the fluorescence transients induced by neural activity. (1) Spike vectors \mathbf{s} were computed by deconvoluting XCaMP-G fluorescence with a constrained non-negative matrix factorization (CNMF).³⁴ (2) The

peak time of fluorescence transients of the XCaMP-G were detected as sampling points when s_{peak} exceeded $\text{mean}(s_{\text{peak}}) + 2 \times \text{SD}(s_{\text{peak}})$, where s_{peak} is all peak values of s , $\text{mean}(x)$ is the average of x and $\text{SD}(x)$ is the standard deviation of x . (3) The onset of the fluorescence transients evoked by neural activity was defined as two frames before the peak time of the fluorescence transients of the XCaMP-G. If multiple fluorescence transients occurred within 3 s, they were excluded from this analysis.

We calculated the area under the curves (AUCs) before 3 s ($\text{AUC}_{\text{before}}$) and AUCs after 3 s ($\text{AUC}_{\text{after}}$) of the fluorescence transients for iBB-GECO1 and XCaMP-G, respectively. We defined $\text{AUC}_{\text{after}}$ exceeding the 97.5% percentile of $\text{AUC}_{\text{before}}$ as a statistically significant change in fluorescence. In addition, we conducted a significance test of the probability distributions of $\text{AUC}_{\text{before}}$ and $\text{AUC}_{\text{after}}$ by the Kolmogorov–Smirnov test.

4.11 | Animal care

For experiments performed at The University of Tokyo, all methods for animal care and use were approved by the institutional review committees of Graduate School of Medicine, The University of Tokyo. Wild-type mice (ICR, Japan SLC) were used. In all the experiments, the mice were housed in a 12 hr-light/12 hr-dark light cycle environment with ad libitum access to food and water.

AUTHOR CONTRIBUTIONS

Rina Hashizume: Data curation (lead); formal analysis (lead). **Hajime Fujii:** Data curation (equal); formal analysis (equal); funding acquisition (equal); writing – review and editing (equal). **Sohum Mehta:** Data curation (equal); formal analysis (equal); writing – review and editing (equal). **Keisuke Ota:** Data curation (equal); formal analysis (equal); writing – review and editing (equal). **Yong Qian:** Data curation (equal); formal analysis (equal). **Wenchao Zhu:** Data curation (equal). **Mikhail Drobizhev:** Data curation (equal); formal analysis (equal); funding acquisition (equal); writing – review and editing (equal). **Jin Zhang:** Funding acquisition (equal); supervision (equal). **Haruhiko Bito:** Funding acquisition (equal); supervision (equal).

ACKNOWLEDGMENTS

The authors thank T. Terai, Y. Kamijo, and S. G. Gandiboina for technical support. Work at the University of Tokyo was supported by the Japan Society for the Promotion of Science (JSPS) Grants-in-Aid KAKENHI (19H05633, 17K13270 to Hajime Fujii, 22H05160, 22H00432, 19H01007, and 17H06312 to Haruhiko Bito), a

Brain/MINDS grant 19dm0207079 from AMED (to Haruhiko Bito), Kato Memorial Bioscience Foundation, Toyota Physical and Chemical Research Institute, Takeda Science Foundation (to Hajime Fujii and Haruhiko Bito), Nakatani Foundation for Advancement of Measuring Technologies in Biomedical Engineering (to Haruhiko Bito), Astellas Foundation for Research on Metabolic Disorders (to Hajime Fujii), and Hitachi Global Foundation (to Haruhiko Bito). Work at University of California, San Diego was supported by the National Institutes of Health, NIH/NCI grant R01 DK073368. Work at the University of Alberta was supported by the Natural Sciences and Engineering Research Council of Canada (NSERC) and the Canadian Institutes of Health Research (CIHR). Work at Montana State University was supported by the National Institutes of Health, NIH/NINDS grant U24 NS109107.

CONFLICTS OF INTEREST

The authors declare no competing interests.

ORCID

Sohum Mehta  <https://orcid.org/0000-0003-4764-8579>
Yong Qian  <https://orcid.org/0000-0001-7849-9022>
Yusuke Nasu  <https://orcid.org/0000-0002-3193-9104>
Jin Zhang  <https://orcid.org/0000-0001-7145-7823>
Haruhiko Bito  <https://orcid.org/0000-0001-6315-9594>
Robert E. Campbell  <https://orcid.org/0000-0003-0604-092X>

REFERENCES

- Greenwald EC, Mehta S, Zhang J. Genetically encoded fluorescent biosensors illuminate the spatiotemporal regulation of signaling networks. *Chem Rev*. 2018;118:11707–11794.
- Nasu Y, Shen Y, Kramer L, Campbell RE. Structure- and mechanism-guided design of single fluorescent protein-based biosensors. *Nat Chem Biol*. 2021;17:509–518.
- Hilderbrand SA, Weissleder R. Near-infrared fluorescence: Application to in vivo molecular imaging. *Curr Opin Chem Biol*. 2010;14:71–79.
- Qian Y, Piatkevich KD, Mc Larney B, et al. A genetically encoded near-infrared fluorescent calcium ion indicator. *Nat Methods*. 2019;16:171–174.
- Qian Y, Cosio DMO, Piatkevich KD, et al. Improved genetically encoded near-infrared fluorescent calcium ion indicators for in vivo imaging. *PLoS Biol*. 2020;18:e3000965.
- Yu D, Baird MA, Allen JR, et al. A naturally monomeric infrared fluorescent protein for protein labeling in vivo. *Nat Methods*. 2015;12:763–765.
- Subach OM, Barykina NV, Anokhin KV, Piatkevich KD, Subach FV. Near-infrared genetically encoded positive calcium indicator based on GAF-FP bacterial phytochrome. *Int J Mol Sci*. 2019;20:3488.
- Subach OM, Subach FV. GAF-CaMP3-sfGFP, an enhanced version of the near-infrared genetically encoded positive

- phytochrome-based calcium indicator for the visualization of neuronal activity. *Int J Mol Sci.* 2020;21:6883.
9. Shemetov AA, Monakhov MV, Zhang Q, et al. A near-infrared genetically encoded calcium indicator for in vivo imaging. *Nat Biotechnol.* 2021;39:368–377.
 10. Yu D, Dong Z, Gustafson WC, et al. Rational design of a monomeric and photostable far-red fluorescent protein for fluorescence imaging in vivo. *Protein Sci.* 2016;25:308–315.
 11. Baloban M, Shcherbakova DM, Pletnev S, Pletnev VZ, Lagarias JC, Verkhusha VV. Designing brighter near-infrared fluorescent proteins: Insights from structural and biochemical studies. *Chem Sci.* 2017;8:4546–4557.
 12. Inoue M, Takeuchi A, Manita S, et al. Rational engineering of XCaMPs, a multicolor GECI suite for in vivo imaging of complex brain circuit dynamics. *Cell.* 2019;177:1346–1360.e24.
 13. Dana H, Sun Y, Mohar B, et al. High-performance calcium sensors for imaging activity in neuronal populations and microcompartments. *Nat Methods.* 2019;16:649–657.
 14. Depry C, Allen MD, Zhang J. Visualization of PKA activity in plasma membrane microdomains. *Mol Biosyst.* 2011;7:52–58.
 15. Harada K, Ito M, Wang X, et al. Red fluorescent protein-based cAMP indicator applicable to optogenetics and in vivo imaging. *Sci Rep.* 2017;7:7351.
 16. Dalangin R, Drobizhev M, Molina RS, et al. Far-red fluorescent genetically encoded calcium ion indicators. *bioRxiv.* 2020. <https://doi.org/10.1101/2020.11.12.380089>
 17. Wagner JR, Zhang J, von Stetten D, et al. Mutational analysis of *Deinococcus radiodurans* bacteriophytochrome reveals key amino acids necessary for the photochromicity and proton exchange cycle of phytochromes. *J Biol Chem.* 2008;283:12212–12226.
 18. Yang X, Kuk J, Moffat K. Conformational differences between the Pfr and Pr states in *Pseudomonas aeruginosa* bacteriophytochrome. *Proc Natl Acad Sci U S A.* 2009;106:15639–15644.
 19. Loughlin PC, Duxbury Z, Mugerwa TTM, Smith PMC, Willows RD, Chen M. Spectral properties of bacteriophytochrome AM1_5894 in the chlorophyll d-containing cyanobacterium *Acaryochloris marina*. *Sci Rep.* 2016;6:27547.
 20. Auldridge ME, Forest KT. Bacterial phytochromes: More than meets the light. *Crit Rev Biochem Mol Biol.* 2011;46:67–88.
 21. Kobachi K, Kuno S, Sato S, Sumiyama K, Matsuda M, Terai K. Biliverdin reductase-a deficiency brighten and sensitize Biliverdin-binding chromoproteins. *Cell Struct Funct.* 2020;45:131–141.
 22. Deán-Ben XL, Sela G, Lauri A, et al. Functional optoacoustic neuro-tomography for scalable whole-brain monitoring of calcium indicators. *Light Sci Appl.* 2016;5:e16201.
 23. Shu X, Royant A, Lin MZ, et al. Mammalian expression of infrared fluorescent proteins engineered from a bacterial phytochrome. *Science.* 2009;324:804–807.
 24. Strickler SJ, Berg RA. Relationship between absorption intensity and fluorescence lifetime of molecules. *J Chem Phys.* 1962;37:814–822.
 25. Drobizhev M, Makarov NS, Tillo SE, Hughes TE, Rebane A. Two-photon absorption properties of fluorescent proteins. *Nat Methods.* 2011;8:393–399.
 26. Drobizhev M, Molina RS, Callis PR, et al. Local electric field controls fluorescence quantum yield of red and far-red fluorescent proteins. *Front Mol Biosci.* 2021;8:633217.
 27. Luchowski R, Gryczynski Z, Sarkar P, et al. Instrument response standard in time-resolved fluorescence. *Rev Sci Instrum.* 2009;80:033109.
 28. Drobizhev M, Molina RS, Hughes TE. Characterizing the two-photon absorption properties of fluorescent molecules in the 680–1300 nm spectral range. *Bio Protoc.* 2020;10:e3498.
 29. Schneider CA, Rasband WS, Eliceiri KW. NIH image to ImageJ: 25 years of image analysis. *Nat Methods.* 2012;9:671–675.
 30. Fujii H, Inoue M, Okuno H, et al. Nonlinear decoding and asymmetric representation of neuronal input information by CaMKII α and calcineurin. *Cell Rep.* 2013;3:978–987.
 31. Ota K, Oisi Y, Suzuki T, et al. Fast, cell-resolution, contiguous-wide two-photon imaging to reveal functional network architectures across multi-modal cortical areas. *Neuron.* 2021;109:1810–1824.e9.
 32. Oomoto I, Uwamori H, Matsubara C, et al. Protocol for cortical-wide field-of-view two-photon imaging with quick neonatal adeno-associated virus injection. *STAR Protoc.* 2021;2:101007.
 33. Pnevmatikakis EA, Giovannucci A. NoRMCorre: An online algorithm for piecewise rigid motion correction of calcium imaging data. *J Neurosci Methods.* 2017;291:83–94.
 34. Pnevmatikakis EA, Soudry D, Gao Y, et al. Simultaneous denoising, deconvolution, and demixing of calcium imaging data. *Neuron.* 2016;89:285–299.
 35. Wagner JR, Zhang J, Brunzelle JS, Vierstra RD, Forest KT. High resolution structure of *Deinococcus* bacteriophytochrome yields new insights into phytochrome architecture and evolution. *J Biol Chem.* 2007;282:12298–12309.
 36. Gourinchas G, Ettl S, Winkler A. Bacteriophytochromes – from informative model systems of phytochrome function to powerful tools in cell biology. *Curr Opin Struct Biol.* 2019;57:72–83.
 37. Salewski J, Escobar FV, Kaminski S, et al. Structure of the biliverdin cofactor in the Pfr state of bathy and prototypical phytochromes. *J Biol Chem.* 2013;288:16800–16814.

SUPPORTING INFORMATION

Additional supporting information can be found online in the Supporting Information section at the end of this article.

How to cite this article: Hashizume R, Fujii H, Mehta S, Ota K, Qian Y, Zhu W, et al. A genetically encoded far-red fluorescent calcium ion biosensor derived from a biliverdin-binding protein. *Protein Science.* 2022;31(10):e4440. <https://doi.org/10.1002/pro.4440>